Rare Metal Materials and Engineering
Volume 47, Issue 11, November 2018
Online English edition of the Chinese language journal

Available online at www.sciencedirect.com

ScienceDirect

Cite this article as: Rare Metal Materials and Engineering, 2018, 47(11): 3321-3328.

ARTICLE

Preparation of Cladding Billet via Direct Chill Casting Process

Guo Jing[1], **Han Xing**[2], **Teng Yingxue**[1], **Wang Hongbin**[1], **Zhang Haitao**[3], **Nong Deng** [4]

[1] University of Science and Technology Liaoning, Anshan 114051, China; [2] Liaoning Zhongwang Group Co. Ltd., Liaoyang 111003, China; [3] Key Laboratory of Electromagnetic Processing of Materials, Ministry of Education, Northeastern University, Shenyang 100819, China; [4] Guangdong Institute of Materials and Processing, Guangzhou 510651, China

Abstract: A mathematic model was built to describe the cladding casting process and the casting parametric influence on the cladding billet. The effect of casting speed, casting temperature and internal cooling water rate on the casting process performance was discussed. Based on the numerical simulation results, the cladding billet was prepared successfully. Moreover, the model was verified by the temperature measurements during the cladding casting process. The interfacial characteristics were investigated by metallographic examination, energy dispersive spectrometer and universal testing machine. The results show that there is a good agreement between the measured and calculated results. The comprehensively considered casting process is: casting speed 100 mm/min, internal cooling water rate 35 L/min, casting temperature 1020 K (AA4045) and 1000 K (AA3003). Based on the simulation results, the AA4045/AA3003 cladding billet with no defects and Φ140 mm/Φ110 mm in size is fabricated successfully. A diffusion layer with 15 μm in width is formed around the bonding interface. The interfacial bonding strength is 107.3 MPa, higher than that of AA3003, indicating that the two alloys have been bonded metallurgically.

Key words: numerical simulation; cladding billet; casting parameter; experiment verification; contact temperature; diffusion layer

Bimetal composite materials have been used for many years to impart a combination of certain physical properties (e.g. mechanical and corrosive) to the clad sheet that cannot be achieved by a monolithic material[1, 2]. These materials can be conventionally produced by roll bonding[3], diffusion bonding[4], extrusion clad[5], and so on. However, these processes usually have the problems of low bonding strength, low efficiency and high cost. A casting process to prepare clad billets, by contrast, is more efficient and economical than these processes.

Recently, based on direct chill (DC) casting, several novel approaches have been introduced to produce composite ingot. Benedyk[6] introduced Novelis Fusion™ process that made breakthrough in the simultaneous DC casting of multiple aluminum alloy layers for rolling ingot. Marukovich[7] studied the possibility of continuous-casting bimetallic components under the condition of direct connection of metals in a liquid state. Jiang [8] prepared a three-layer composite ingot of 4045/3003/4045 aluminum alloys by a direct chill semi-continuous casting process. However, there are few reports on cladding billet, which are used to prepare condense pipes of automotive engines. The casting parametric influence regularities on the composite interface were rarely studied.

In this paper, a mathematic model was developed to describe the cladding casting process and the casting parametric influence on the cladding billet. By contrasting the calculated and measured results, the mathematic model was experimentally validated and it is accurate and reliable. Based on numerical simulation results, AA4045/AA3003 cladding billet with Φ140 mm/Φ110 mm in size was prepared successfully.

Received date: November 25, 2017
Foundation item: National Natural Science Foundation of China (51374128); the Science and Technology Program of Guangdong, China (2013B010102026, 2013B061800054, 2015B090901044)

Corresponding author: Guo Jing, Ph. D., Senior Engineer, School of Materials and Metallurgy, University of Science and Technology Liaoning, Anshan 114051, P. R. China, Tel: 0086-412-5929557, E-mail: liaokd_guoj@163.com

1 Experiment

In the present study, AA4045 is selected as a clad-layer because of its excellent brazing performance, and AA3003 as a core-layer due to its well corrosion resistance. The chemical composition of the two aluminum alloys is listed in Table 1. The schematic diagram of experiment installation mainly consists of pouring systems, molds, cooling systems and starting head. Initially, the starting head was located in the mold. The core melt was poured into the inner-mold, forming a solid shell (called supporting layer) immediately. Then, the starting head was steadily withdrawn, and the clad melt was fed into the outer-mold at the same time. Through optimizing the casting parameters, the cladding billet, which is in size of *Φ*140 mm/*Φ* 110 mm×1600 mm with perfect surface quality, was prepared.

The specimen in cross section of the cladding billet was etched with 10% NaOH solution. The macro-morphology of them were analyzed. The sample was cut from the interfacial region in the cross section and etched with 0.5% HF solution. In order to investigate the interfacial characteristics, metallographic examination and Energy Dispersive Spectrometer (EDS) were used. Tensile tests were performed using a universal testing machine. All the results were averaged.

2 Mathematical Model and Experiments of the Cladding Casting

In terms of the treatment of the latent heat, there are two main methods, namely, the equivalent specific heat and enthalpy methods. In this model, the first method was used to model accurately energy transport during the solidification process. In this research, a single domain volume-average model is introduced to describe the cladding casting process and the geometrical model, boundary conditions and mesh are shown in Fig.1. All these regions are implicitly defined within the system by distributions of energy determined from the solutions model equations. The interfacial region and the region close to the mold are the key regions of heat transfer and melt flowing, so finer mesh is set in these regions and coarse mesh in other regions, as shown in Fig.1b. All the grids are hexahedral.

In order to improve the calculation speed, only half of the cladding billet is used symmetrically and some assumptions are given as follows:

Table 1 Chemical composition of the alloys (wt%)

Alloy	Si	Fe	Cu	Mn	Mg	Zn	Ti	Al
AA4045	9~11	0.8	0.3	0.05	0.05	0.1	0.2	Bal.
AA3003	0.6	0.7	0.05~0.2	1.0~1.5	-	0.1	-	Bal.

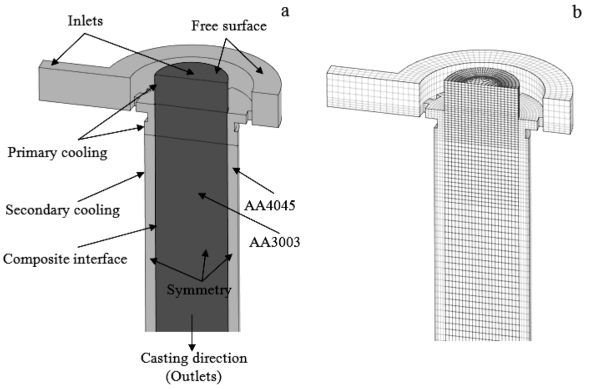

Fig.1 Geometrical model, boundary conditions (a) and mesh (b) for cladding casting

(1) In this model, the calculation about the solute field is not included in the research;

(2) In this model, the molten aluminum alloys behave as an incompressible fluid, so the density of the melt is the constant. But the thermal buoyancy must be included in this model; therefore the Boussinesq approximation is used to calculate the thermal buoyancy and is expressed as:

$$F_{\mathrm{thermal}}=\rho g\beta(T-T_0) \tag{1}$$

Where ρ and β are the density and the volume expansion coefficient of the molten aluminum, respectively, T_0 is the reference temperature and is frequently given as the temperature when the dendrite coherence occurs.

During cladding casting process, the solidified part moves along the axial with casting speed.

In this research, a single domain volume-average model is used. All these regions are implicitly defined within the system by distributions of energy determined from the solutions model equations, which are written as follows:

Conservation equation of mass:

$$\nabla\cdot U=0 \tag{2}$$

Conservation equation of momentum:

$$\nabla\cdot(\rho UU)=\nabla\cdot(\mu_{\mathrm{eff}}\nabla U)-\nabla P+S_{\mathrm{m}} \tag{3}$$

Conservation equation of energy:

$$\nabla\cdot(\rho UT)=\nabla\cdot\left(\frac{k}{c_{\mathrm{p}}}\nabla T\right)+S_{\mathrm{th}} \tag{4}$$

In the Eq.(2), ∇ is gradient operator, U is velocity vector. In Eq.(3), ρ, μ_{eff} and S_{m} are melt density, effective viscosity and momentum source, respectively. The effective viscosity μ_{eff} is given by $\mu_{\mathrm{eff}}=\mu_{\mathrm{l}}+\mu_{\mathrm{t}}$, where μ_{l} is laminar viscosity in the liquid and μ_{t} is turbulent viscosity. The momentum source S_{m} includes thermal buoyancy and Darcy source term. In Eq.(4), S_{th} is thermal source, i.e., latent heat of solidification. k is the turbulence kinetic energy, C_{p} is specific heat capacity, T is melt temperature.

Modeling of fluid flow in the mushy region and treatment of the conservation equations in the solid region are carried out by different viscosity and permeability in different regions. In most models, the Darcy model is usually used. However, when the solidification of equiaxed grains is considered, particularly, in the early stage of solidification when the solid fraction is small, the equiaxed grains will move freely with the liquid, so the Darcy flow is not important. Darcy flow becomes significant when dendrite coherency occurs, that is, when a rigid dendrite skeleton is established. In addition, a velocity towards casting direction is exerted on the whole alloys.

In this model, the standard k-ε model, which is a semiempirical model, is used to model transport of turbulence kinetic energy (k) and its dissipation rate (ε). The first form of this model was proposed by Harlow and Nagayama and suggested that:

$$\mu_t = \rho C_\mu \frac{k^2}{\varepsilon} \tag{5}$$

Where C_μ is a function of the turbulent Reynolds number which is a constant value; k and ε is the turbulence kinetic energy and its rate of dissipation, respectively, and obtained from the following transport equations:

$$\nabla \cdot (\rho U k) = \nabla \left(\mu_1 + \frac{\mu_t}{\sigma_k} \right) + G_k - \rho\varepsilon - \frac{\mu_1}{K + x} k \tag{6}$$

$$\begin{aligned}\nabla \cdot (\rho U \varepsilon) = \nabla \left[\left(\mu_1 + \frac{\mu_t}{\sigma_\varepsilon} \right) \nabla_\varepsilon \right] + C_1 \frac{\varepsilon}{k} G_k - \\ C_2 \rho \frac{\varepsilon^2}{k} - \frac{\mu_1}{K + x} \varepsilon\end{aligned} \tag{7}$$

Where, K and x are permeability and very small positive number to avoid diverging of conversation equations, respectively, respectively. Permeability K is given as a function of solid fraction f_s, i.e., $K=K_0(1-f_s)^3/f_s^2$. Where K_0 is initial permeability. G_k represents the generation of turbulence kinetic energy due to the mean velocity gradients, calculated as follows: $G_k=-\rho\mu'\mu_j'(\partial\mu_j/\partial x_i)$. C_1 and C_2 are constants. σ_k and σ_ε are the turbulent Prandtl number for k and ε, respectively. ∇_ε is gradient operator for ε. All constants, which are used in the model, are listed in Table 2.

The thermophysical and other material properties of the alloys used during the calculation procedure are listed in Table 3. The thermal properties of the alloys were calculated by JMat-Pro, and the results of specific heat, thermal conductivity and fraction solid were shown in Fig.2, Fig.3 and Fig.4. In our former work[9], the boundary conditions are set in detail and the parameters are list in Table 4.

3 Results and Discussion

3.1 Verification of the mathematic model

In order to verify the accuracy of above-built mathematic model, the interfacial temperature was measured during cladding casting. The thermocouples were vertically fixed to the stainless steel rods installed in the starting head and moved down with the lowering of the starting head. These K-type thermocouple was linked to a data logger (resolution, 0.001 °C) to record the temperatures every 0.2 s. When the casting was finished, the corresponding temperature data was transferred to a personal computer and then processed to yield a Distance-Temperature plot.

Table 2 Constants used in k-ε model

C_1	C_2	σ_k	σ_ε	C_μ
1.44	1.92	1.0	1.3	0.09

Table 3 Physical properties and constant used in the numerical simulation

Physical properties	AA3003	AA4045
Density, ρ/kg·m^{-3}	2520	2420
Liquidus temperature, T_l/K	931	868
Solidus temperature, T_s/K	918	850
Latent heat of fusion, L/×10^5 J·kg^{-1}	3.9	4.7
Volume expansion coefficient, β/K^{-1}	6.7×10^{-5}	5.2×10^{-5}
The initial permeability, K_0/×10^{-11}	2	2
Solid fraction of dendrite contact, f^*	0.3	0.25
Reference temperature, T_0/K	925	842

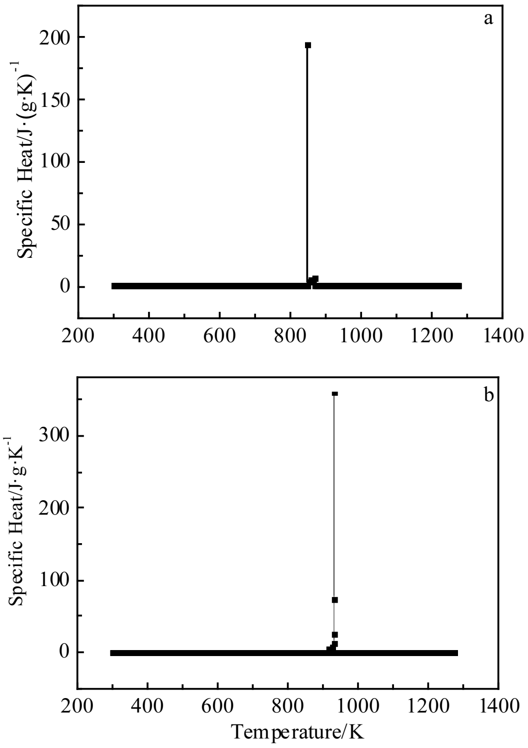

Fig.2 Specific heat of the two aluminum alloys: (a) AA3003 and (b) AA4045

The result is shown in Fig.5. It reveals that there is a well

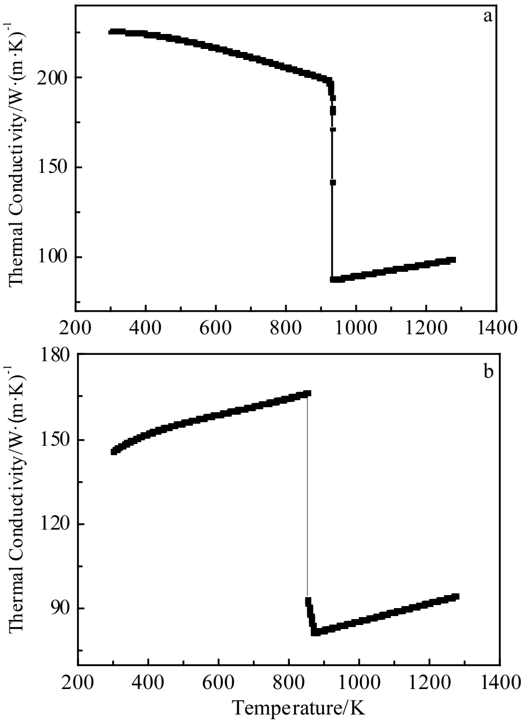

Fig.3 Thermal conductivity of the two aluminum alloys: (a) AA3003 and (b) AA4045

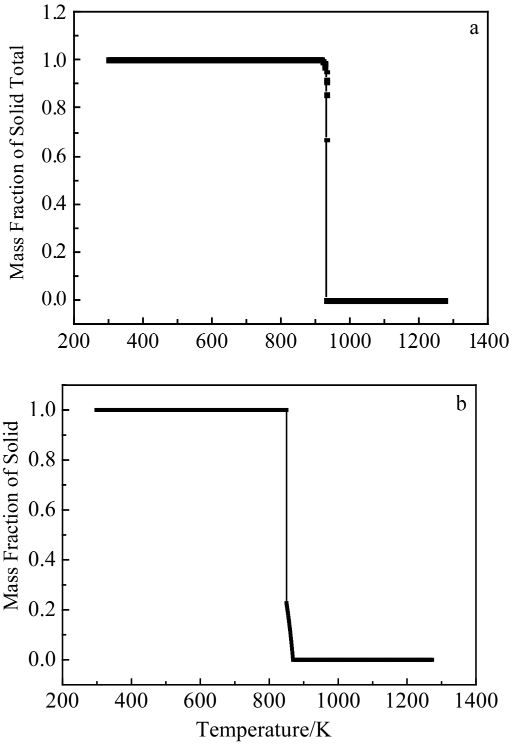

Fig.4 Fraction solid of the two aluminum alloys: (a) AA3003 and (b) AA4045

Table 4 Boundary conditions for flow inlet and outlet

Boundary	Inlet_{3003}	Inlet_{4045}	Outlet_{3003}	Outlet_{4045}
Velocity/mm·min^{-1}	$V_{\text{cast}}(S_{\text{inlet}}/S_{\text{outlet}})$	$V_{\text{cast}}(S_{\text{inlet}}/S_{\text{outlet}})$	80~120	80~120
Temperature/K	1000	1000~1040	300	300
Turbulent kinetic energy/J	$k=0.01V^2_{\text{inlet}}$	$k=0.01V^2_{\text{inlet}}$	0	0
Turbulent dissipation rate	$\varepsilon=k^{1.5}/R_{\text{noz}}$	$\varepsilon=k^{1.5}/R_{\text{noz}}$	0	0

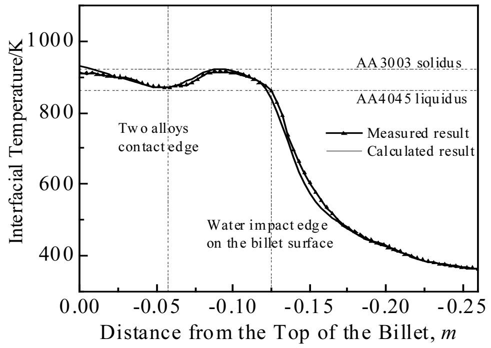

Fig.5 Comparison between the measured and calculated variation of interfacial temperature

agreement between the measured and simulated results. With the cooling of inner-mold, the surface temperature of the supporting layer decreased gradually until the AA4045 melt contacted with it. Then the interfacial temperature increased because the supporting layer was reheated by the AA4045 melt. Subsequently, the interfacial temperature decreased rapidly due to the cooling of outer-mold and secondary cooling water. As seen, at the interfacial region, the supporting layer was solid-state and the AA4045 remained liquid between the two alloys contact edge and the water impact edge, accelerating the diffusion of alloy elements across the interface.

3.2 Effect of casting speed on temperature field around the interface

Fig.6 shows the temperature fields at different casting speeds, 80, 100 and 120 mm/min. Obviously, the supporting layer is reheated by AA4045 melt, namely backheating phenomenon. The sump deepens, the supporting layer thickens and the interfacial temperature increases with the increasing of casting speed. In order to investigate and illuminate clearly the effect of casting speed on interfacial temperature field during the cladding casting process, the interfacial temperature data is extracted, as shown in Fig.7. When casting speed is 80 mm/min, the contact temperature is only 840 K, lower than that of AA4045 solidus, resulting in that AA4045 melt starts to solidify before contacts with the

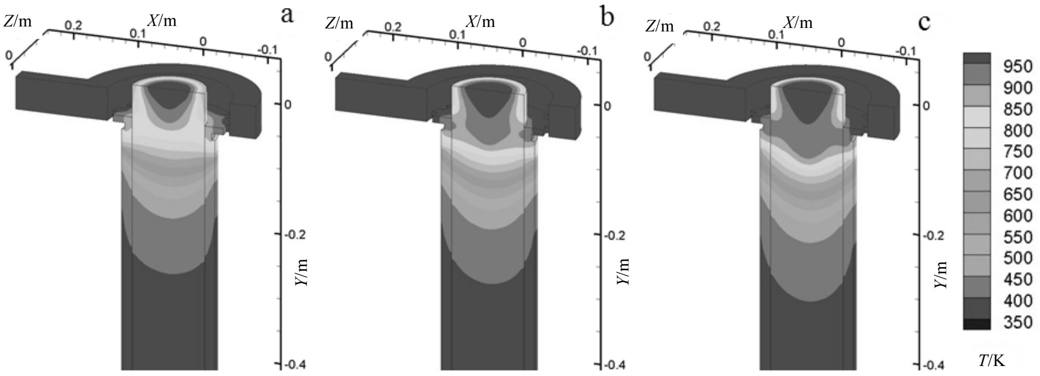

Fig.6 3D-surface plot of temperature contours under different casting speeds: (a) 80 mm/min, (b) 100 mm/min, and (c) 120 mm/min

supporting layer. However, if the casting speed reaches 120 mm/min, the contact temperature is close to AA3003 solidus, and then the interfacial temperature exceeds it resulting in the back heating phenomenon. It is very likely that the two alloys are mixed in this case. When the casting speed is 100 mm/min, the contact temperature stays near the AA3003 solidus, but will not exceed it. Therefore, an appropriate casting speed is 100 mm/min.

3.3 Effect of casting temperature on the temperature field around the interface

The 3D-surface plots of temperature field at different casting temperatures (1000, 1020, 1040 K), are shown in Fig.8. Fig.9 shows the variation of interfacial temperature at different casting temperatures. It can be seen that the interfacial temperature field is almost unchanged along with casting temperature enhancement, as well as the sump depth and the supporting layer thickness. It can reveal that casting temperature hardly affects the temperature field.

These are due to that the enhancive sensible heat of temperature rise is far less than the latent heat of crystallization. The sensible heat of the casting temperature increased T_i (20 $^{\circ}$C):

$$Q_s = mcT_i \tag{8}$$

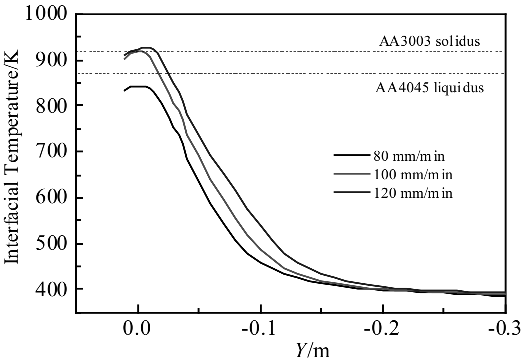

Fig.7 Variation of interfacial temperature at different casting speeds

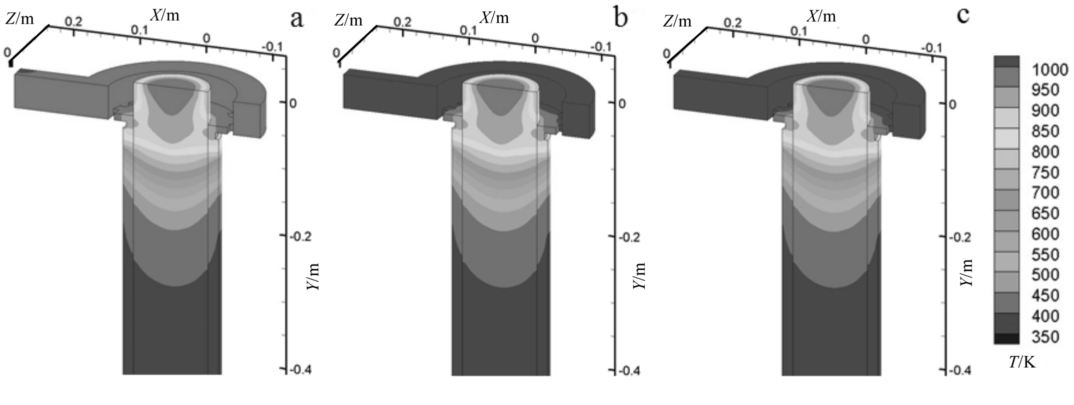

Fig.8 3D-surface plot of temperature contours at different casting temperatures: (a) 1000 K, (b) 1020 K, and (c) 1040 K

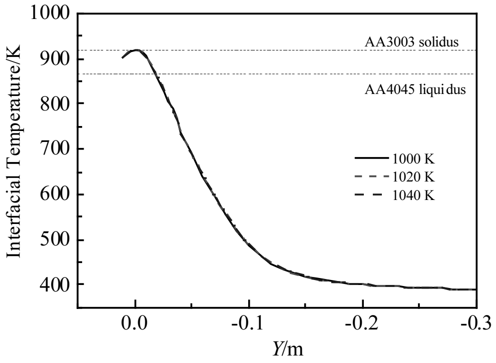

Fig.9 Variation of interfacial temperature at different casting temperatures

where m is the quality of alloy, c is specific heat capacity of 4045 aluminum alloy 1170 J·(kg·K)$^{-1}$.

However, the latent heat that the alloy released when solidified (4.7×105 J·kg^{-1})

$$Q_\text{L}=mL \tag{9}$$

Where L is the crystallization latent heat per unit mass of AA3003.

Compare Q_S and Q_L,

$$\frac{Q_\text{S}}{Q_\text{L}}=\frac{mcT_i}{mL}=\frac{cT_i}{L}=0.0025 \tag{10}$$

Thus it can be seen that the quantity of heat, which is caused by the increasing of casting temperature from 1000 to 1040 K, is much smaller than the crystallization latent. Consequently, casting temperature has little effect on the interfacial temperature field. However, a higher casting temperature contributes to improvement in AA4045 liquidity and the billet surface quality.

3.4 Effect of internal cooling on the temperature around the interface

Fig.10 shows the predicted distribution of temperature field for internal cooling water ranging between 20 and 40 L/min. As seen, the increasing of internal cooling water rate facilitates the supporting layer formation. In order to determine the internal cooling water rate, the interfacial temperature data was extracted to plot curves, as shown in Fig.11. The contact temperature increases with decreasing internal cooling water rate. A lower internal cooling water rate is conducive to increase the contact temperature, thereby creating a strong bond at the interface. However, when the internal cooling water rate is reduced to 20 L/min, the backheating phenomenon will make the interfacial temperature over AA3003 solidus, which may lead to the excessive remelting of the supporting layer. Therefore, to obtain a strong bond between the two alloys, but without excessive remelting of the supporting layer, the internal cooling water rate should be around 30L/min.

3.5 Comprehensive parametric influence on the cladding billet

From the above analysis, the casting speed and the internal cooling water rate are more significant than the casting temperature for interface bonding. In order to investigate the comprehensive influence of casting parameters on the cladding billet, temperature difference with different casting speeds and internal cooling water rates is plotted as shown in Fig.12. The temperature difference between contact temperature and AA3003 solidus is set as ΔT, which ranges appropriately from 0 to 55 K. If ΔT is below or above the range, it can lead to the separation of the two alloys (as shown in the black region of Fig.12) or the excessive remelting of the supporting layer (as shown in the red region of Fig.12), respectively.

Therefore, the comprehensively considered casting process is: casting speed is 100 mm/min, internal cooling water rate is 35 L/min, casting temperature are 1020 K (AA4045) and 1000 K (AA3003).

3.6 Experiment result

Based on the numerical simulation results, the cladding billet was fabricated successfully. The photograph of cladding

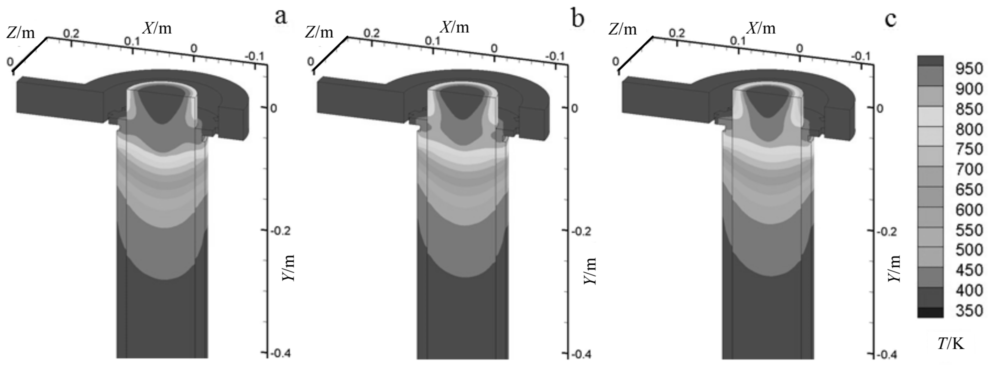

Fig.10 3D-surface plot of temperature field with different internal cooling water rates: (a) 20 L/min,(b) 30 L/min, and (c) 40 L/min

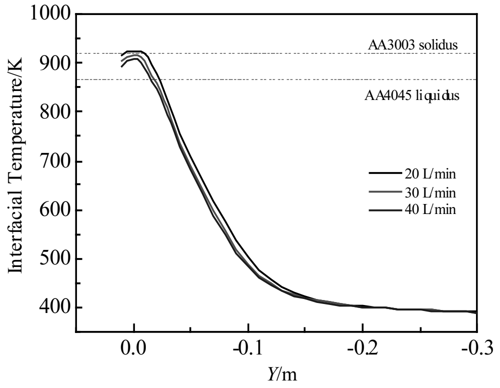

Fig.11 Variation of interfacial temperature with different internal cooling rates

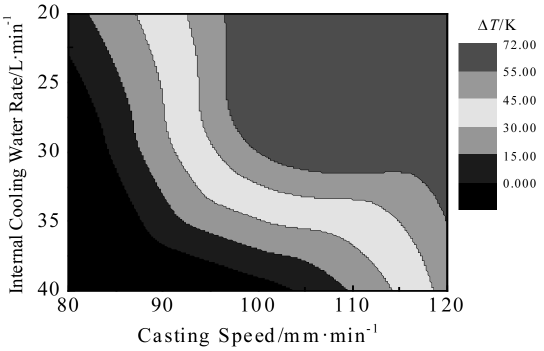

Fig.12 Comprehensive influence of the casting speed and the internal cooling water rate

billet, macrostructure and interfacial microstructure in cross section are shown in Fig.13. The two different alloys are separated apparently into two parts by the interface without any discontinuity or pores, as shown in Fig.13b. For the AA4045 side, the microstructure contains dendritic α-Al phase and needlelike eutectic silicon, and in the AA3003 side, a few Al_6Mn particles are distributed homogeneously in the Aluminum matrix, as shown in Fig.13c.

Fig.14 shows the distribution of elements across the interface measured by EDS. It can be seen that the content of Si element decreases gradually from the AA4045 side to the AA3003 side, while the content of Mn element increases across the interface. A diffusion layer in width of 15 μm was formed by the interdiffusion of the element during the cladding casting process.

Tensile test is an effective way to examine the interface bond strength. The original tensile sample and the fractured sample are shown in Fig.15. Tensile test shows that the mean value of the samples is 107.3 MPa, which is close to the ultimate tensile strength of AA3003. The fracture locates in the AA3003 side, while the interface remains well. It is confirmed that the bonding of the two alloys belongs to metallurgical bonding.

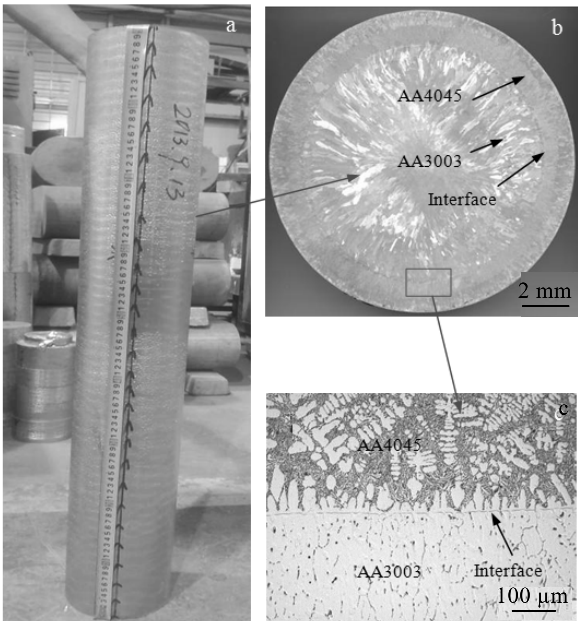

Fig.13 Photograph of the cladding billet (a), macrostructure (b) in cross section, and interfacial microstructure (c)

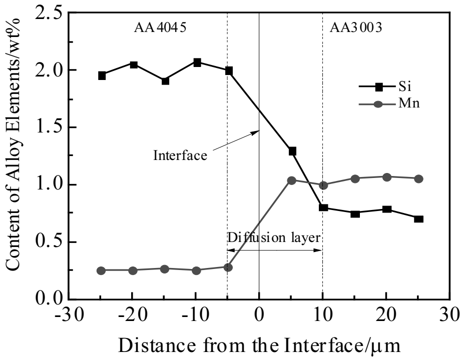

Fig.14 Distribution of elements across the interface

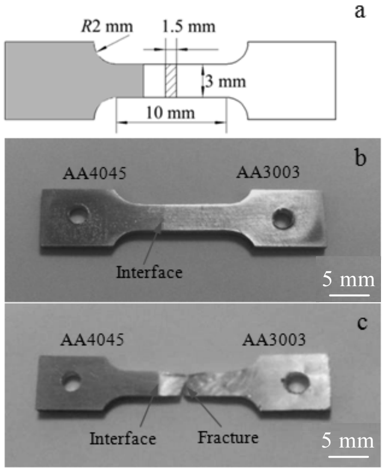

Fig.15 Tensile size (a), original (b), and fractured (c) samples

4 Conclusions

1) A mathematic model to describe the cladding casting process and the casting parametric influence on the cladding billet is presented. The model is used to simulate the casting process of AA4045/AA3003 cladding billet using various casting speeds, casting temperatures and internal cooling water rates.

2) The simulation results prove to be promising in identifying the potential pitfalls in the process. When casting speed reaches 120 mm/min or internal cooling rate decreases to 20 L/min, excessive remelting would occur around the interface. A lower casting speed (80 mm/min or lower) would lead to the separation of the two alloys. In addition, casting temperature has little effect on the interfacial temperature field.

3) The comprehensively considered casting process is: casting speed is 100 mm/min, internal cooling water rate is 35 L/min, casting temperature are 1020 K (AA4045) and 1000 K (AA3003).

4) Based on the simulation results, the AA4045/AA3003 cladding billet with no defects in size of Φ140 mm/Φ110 mm is fabricated successfully. Si and Mn elements diffuse across the interface and form a diffusion layer in width of 15 μm. The interfacial bonding strength is 107.3 MPa, and it is higher than that of AA3003.

References

1 Gupta A, Lee S T, Wagstaff R B. *Materials Technology*[J], 2007, 22: 71

2 Guo X Z, Fan M Y, Liu Z L *et al. Rare Metal Materials and Engineering*[J], 2017, 46(5): 1192

3 Talebian M, Alizadeh M. *Materials Science and Engineering A*[J], 2014, 590: 186

4 Zhang J, Luo G Q, Wang Y Y *et al. Materials Letters*[J], 2012, 83: 189

5 Rhee K Y, Han W Y, Park H J *et al. Materials Science and Engineering A*[J], 2004, 384: 70

6 Benedyk J C. *Light Metal Age*[J], 2006, 64: 48

7 Marukovich E I, Branovitsky A M, Na Y S *et al. Materials and Design*[J], 2006, 27: 1016

8 Jiang H X, Zhang H T, Qin K *et al. Transaction Nonferrous Metal Society China*[J], 2001, 21: 1692

9 Zhang H T, Nagaumi H, Zuo Y B *et al. Materials Science and Engineering A*[J], 2007, 448: 189

DC 铸造法制备包覆铸锭研究

郭 菁[1]，韩 星[2]，藤莹雪[1]，王洪斌[1]，张海涛[3]，农 登[4]

(1. 辽宁科技大学，辽宁 鞍山 114051)

(2. 辽宁忠旺集团有限公司，辽宁 辽阳 111003)

(3. 东北大学 材料电磁过程研究教育部重点实验室，辽宁 沈阳 110819)

(4. 广东省材料与加工研究所，广东 广州 510651)

摘 要：首先建立了一个数学模型，用来模拟包覆 (direct chill, DC)铸造过程和工艺参数（包括铸造速度、铸造温度、冷却水量）对包覆铸锭的影响规律。以模拟结果为依据，通过优化工艺参数成功制备了尺寸为 Φ140 mm/Φ110 mm 的 AA4045/AA3003 包覆铸锭，并通过实验测温对模型进行了验证。采用多种手段对界面的组织性能进行了检测。结果表明，测温结果与模拟结果相互吻合，模型可靠。优化后的包覆铸造工艺参数为：铸造速度 100 mm/min，冷却水量 35 L/min，铸造温度 1020 K（AA4045）、1000 K（AA3003）。包覆铸锭界面处无气孔、夹杂等缺陷，通过元素扩散形成了约 15 μm 的扩散层。界面抗拉强度为 107.3 MPa，大于 AA3003 合金基体强度，说明 2 种合金实现冶金结合。

关键词：数值模拟；包覆铸锭；铸造参数；实验验证；接触温度；扩散层

作者简介：郭 菁，男，1982 年生，博士，高级工程师，辽宁科技大学材料与冶金学院，辽宁 鞍山 114051，电话：0412-5929557, E-mail: liaokd_guoj@163.com